Acoustic Delay Lines to Measure Piezoelectricity in 4H Silicon Carbide

Pen-Li Yu and Sunil A. Bhave
OxideMEMS Lab, Purdue University
West Lafayette, IN, 47907, USA
yu586@purdue.edu

This paper reports the first measurement of the electromechanical coupling coefficient (K^2) for the Rayleigh wave in 4H polytype of Silicon Carbide (SiC). We fabricate 18 acoustic delay lines on two 4H SiC chips. Transmitted acoustic signals are measured at 423 MHz and 676 MHz for devices with 16 μm and 10 μm wavelength, respectively. We post-process the transmitted signal in time-domain to isolate the surface acoustic wave transmission. From the filtered signals we extract K^2 to be (0.93±0.05) ×10^{-4} % and (0.66±0.02) ×10^{-4} % at 423 MHz and 676 MHz.

Keywords—Silicon Carbide; Piezoelectric coupling coefficient; Surface acoustic wave; Acoustic delay line; Time-domain analysis.

I. INTRODUCTION

Color centers in wide-bandgap semiconductor crystal have emerged as a promising quantum resource with applications in quantum computing and quantum sensing [1]. The localized electrons in the defects host room-temperature spin states with analogous properties to atoms trapped in vacuum. Interaction between these spin states and strain field open the prospects of control and readout these spin quantum bits (qubits) with resonant piezoelectric nano- and micro-electromechanical devices (NEMS and MEMS) [2]–[6]. MacQuarrie et al. [3] demonstrated that to control these defect spins in a non-piezoelectric semiconductor such as diamond, one can fabricate a piezoelectric transducer on the substrate to generate large oscillation stress [7]. In contrast to this approach, discovering a piezoelectric semiconductor crystal that hosts defect spins could add flexibility and scalability to the design of hybrid quantum devices.

A piezoelectric potential can be created in a binary crystal with non-inversion symmetry, such as zincblende and wurtzite crystal structures. In these crystals, ions are polarized under applied stress and strain. The wurtzite structure is commonly found to host the strongest piezoelectric semiconductors, such as GaN, AlN, and ZnO. Recently, 4H and 6H silicon carbide (SiC), SiC polytypes with wurtzite structure, were found to host coherent spin states in vacancy defects at room temperature [8]. 6H SiC has been reported to have weak piezoelectricity in 1965 [9] and 1989 [10]. In Ref. [10], the authors report the electromechanical coupling factor k_{31}^2 of 6H SiC to be k_{31}^2=9.8×10^{-2} % measured using a resonator. However, the electromechanical coupling factor for 4H SiC has not been characterized yet.

We report the first measurement on K^2 for the Rayleigh wave of 4H SiC using acoustic delay lines. We measure K^2 of (0.93±0.05) ×10^{-4} % and (0.66±0.02) ×10^{-4} % at 423 MHz and 676 MHz, respectively. This level of piezoelectricity, although relatively weak, together with its ultra-high Q-frequency product [7, 10], could allow mechanical control of the ground state spin triplet in 4H SiC [12].

II. DESIGN OF EXPERIMENT

We employ surface-acoustic-wave delay lines on a 4H SiC substrate to measure K^2 of the Rayleigh wave. The delay line consists of a pair of interdigital transducers (IDTs). It introduces a time delay to an applied signal through generation, propagation, and detection of the surface acoustic wave (SAW) on a piezoelectric substrate. The transmission scattering parameter S_{21} contains a term proportional to K^2 and is delayed by travel time of the SAW.

Along with the SAW transmission, there is also RF feedthrough due to capacitive coupling between the two ports. Ideally, the RF feedthrough should be minimized by optimizing the IDT which makes the feedthrough negligible. However, for weak piezoelectric substrate such as 4H SiC, the SAW contribution is smaller than the RF feedthrough background.

In this measurement, we perform inverse short-time Fourier transform (inverse STFT) to separate the RF feedthrough and SAW transmission in time-domain. This is feasible because the RF feedthrough travels close to the speed of light while the SAW travels at the Rayleigh wave speed. We filter out the RF feedthrough and convert the SAW signal back to frequency domain with STFT. K^2 can then be extracted from the filtered spectrum by the Mason model [13]

$$K^2 = \frac{1 + \left[R_g 2\pi f C_T\right]^2}{2\alpha\pi R_g C_T f_0 N_p} \widetilde{S_{21}}(f_0) \qquad (1)$$

Here, K^2 is defined by $2(V_{Sf} - V_{Sm})/V_{Sf}$, where V_{Sf} (V_{Sm}) is the velocity of the free surface (metalized surface), $\widetilde{S_{21}}(f_0)$ is the filtered signal S_{21}, $f_0 = V_{Sf}/\lambda = V_{Sf}/2p$ is the fundamental center frequency of the SAW, λ is the acoustic wavelength, p is the IDT pitch, α=2.87 for solid-electrode with 0.5 metallization ratio, N_p is the number of electrode pairs, C_T is the static total IDT capacitance. In equation (1), we assume that the acoustic attenuation in the delay length of interest is negligible for determining K^2.

We use a high-purity semi-insulating 4H SiC wafer with 4" diameter and 500 μm thickness from Cree Inc. The crystal is

<0001> oriented within 0.2°. The resistivity is 10^9 ohm-cm. The wafer is diced into 1 cm square chips. Based on the measurement scheme, we design IDTs with different apertures and delay lengths. The design parameters are summarized in Table I. We fabricate 18 delay lines with 8 μm and 12 μm pitches on two chips (Fig. 1) using contact photolithography and a lift off process. The IDTs have solid-electrodes with 190 nm/10 nm Aluminum/Titanium. Aluminum is chosen to avoid internal reflection between the IDT fingers.

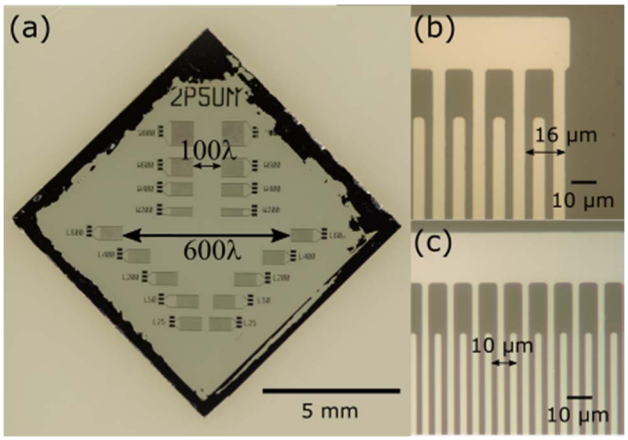

Fig. 1. Photographs of the fabricated acoustic delay lines on the 4H SiC substrates. (a) Nine delay lines with 5 μm pitch on a 1cm x 1cm SiC chip. The top four devices have a fixed IDT separation of 100 wavelength and four different apertures while the lower five devices have a fixed aperture of 400 μm and five different delay lengths. See Table I for the device parameters. The delay lines are 45° off from the chip edges to avoid reflected surface acoustic wave from the edges. (b)-(c) Photos of solid-electrode IDTs with 8 μm and 5 μm pitch, respectively.

TABLE I. DESIGN PARAMETERS OF THE SIC DELAY LINES

IDT pitch (p=λ/2)	8 μm, 5 μm
IDT pairs (N_p)	80
IDT aperture (W)	800, 600, 400, 200 μm
IDT separation (L_0)	600λ, 400λ, 200λ, 50λ, 25λ, 10λ

III. MEASUREMENT AND ANALYSIS

We measure the calibrated S parameters (S_{11}, S_{12}, S_{21}, and S_{22}) of all the acoustic delay lines using a network analyzer. The SAW velocity is reported to be 6832 m/s [14], and hence SAW signals for devices with 16 μm and 10 μm are expected to be at 427.0 MHz and 683 MHz, respectively. For each device, we analyze the amplitude and phase of S_{21}. In Fig. 2, we plot one of the measured S_{21} amplitude and phase spectrum (see Fig. 2 caption for device parameters). In Fig. 2 (a), we see a small peak with amplitude ripples at the expected frequency. On the other hand, the phase spectrum shown in Fig. 2 (b) has a cleaner SAW signature. We observe that the phase is linearly decreasing with frequency between 421 to 426 MHz, indicating the time delay due to SAW.

The device corresponding to the measurements in Fig. 2 has a delay length L, the distance between the centers of two IDTs:

$$L_0 + \frac{L_{\mathrm{IDT1}}}{2} + \frac{L_{\mathrm{IDT2}}}{2} = (400 + 40 + 40)16\ \mu\mathrm{m} = 7.68\ \mathrm{mm}$$

where L_0 is the IDT separation and $L_{\mathrm{IDT1(2)}}$ is the length of the first (second) IDT length. Hence the designed delay time is 7.68mm/(6832m/s) = 1.12 μs.

From the phase data between 421 MHz and 426 MHz, we extract a delay time by calculating the slope:

$$\tau = \frac{d\theta}{df}\frac{1}{360^o} = 1.15\ \mu s.$$

The number agrees well with the designed delay time. This proves that surface acoustic waves are generated and prorogated.

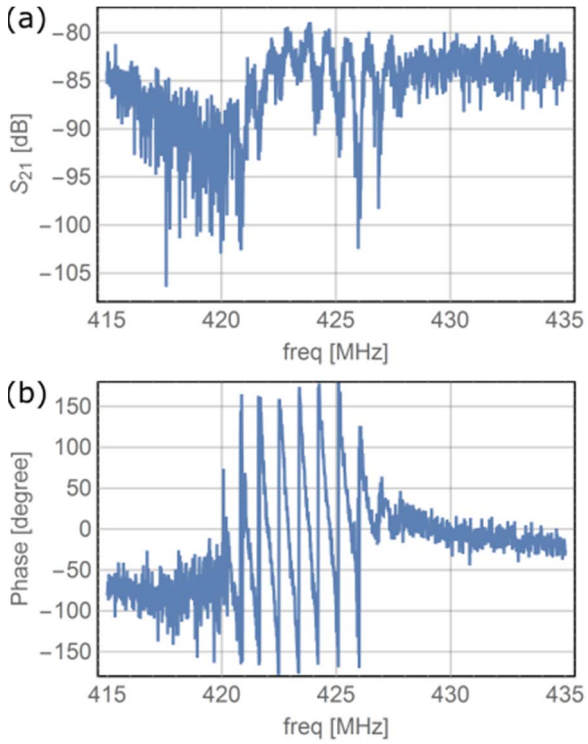

Fig. 2. Measured delay-line transmission signals. The device parameters are (p, N_p, W, L_0) = (8 μm, 80, 400 μm, 400 λ). (a) Magnitude of S_{21}. A small peak with amplitude fluctuation is visible in the 421-426 MHz range. (b) Phase of S_{21}. The negative slope of phase in the 421-426 MHz indicates a SAW delay time of 1.15 μs. This number is consistent with the expected 1.12 μs delay time.

We then perform the inverse STFT to convert the signal to time domain and plot two groups of data in Fig. 3. In Fig. 3 (a), we plot the S_{21} in time domain for devices with delay lengths (time) of 7.68 mm (1.12 μs), 4.48 mm (0.66 μs), 2.08 mm (0.30 μs), and 1.68mm (0.25 μs). For each data, we observe a RF feedthrough signal around 0s and a SAW signal at the expected delay time. In Fig. 3 (b), we plot the S_{21} in time domain for devices with the same delay length (time) of 2.88 mm (0.42 μs) and different apertures. We see that all SAW signals center at the expected delay time. Note that the SAW peaks at various delay time have the same amplitude. This verifies the assumption of Eq. 1 that the acoustic attention is negligible.

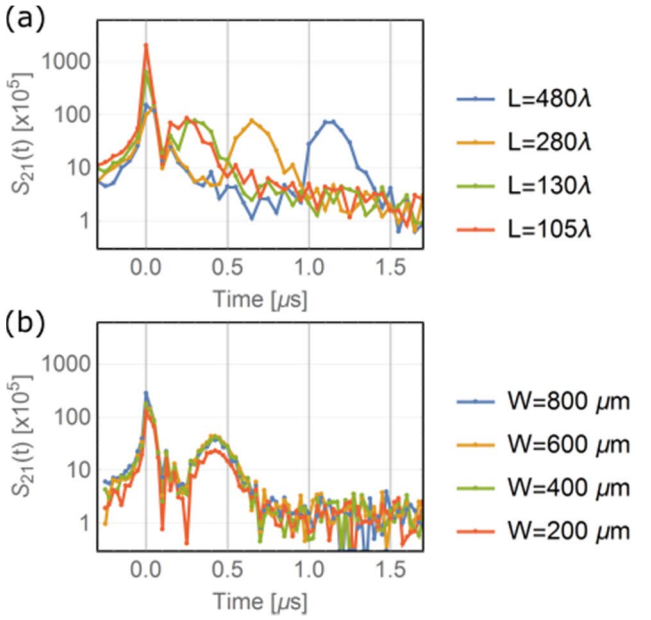

Fig. 3. Transmission signals in time domain [S_{21}(t)] for two groups of devices. For each data there are a RF feedthrough peaked around 0s and a second set of SAW signals peaked around their expected delay times. (a) Magnitude of S_{21}(t) as a function of time for four devices with different IDT separation L_0=400 λ, 200 λ, 50 λ, 25 λ. The fixed parameters are (p, N_p, W) = (8 μm, 80, 400 μm). The expected delay time for these devices are 1.12 μs, 0.66 μs, 0.30 μs, 0.25 μs, respectively. (b) Magnitude of S_{21}(t) for four devices with a common IDT separation L_0 = 100 λ, p = 8 μm, N_p = 80, and four different apertures W=800, 600, 400, 200 μm. The expected delay time is 0.42 μs. The SAW signals are relatively the same except for the W=200 μm device.

Since we can reliably detect the SAW in 4H SiC in time domain, we can filter out the RF feedthrough and isolate the SAW signals. We then perform STFT to transform time-domain SAW signals back to frequency domain. In Fig. 4, we plot two filtered signals in frequency domain. We can see that the background is greatly reduced (at least -20 dB reduction), and the remaining signals closely follow the shape of sinc function. As another check, we fit the filtered signals with the Mason model and find good agreement especially in the main lobe bandwidth. We then use Eq. 1 to extract K^2. We apply this time-domain filtering technique to all the data. The average K^2 is found to be (0.93±0.05)×10^{-4} and (0.66 ±0.02)×10^{-4} at 427 MHz and 676 MHz devices, respectively. The result is summarized in Table II.

TABLE II. SUMMARY OF THE MEASUREMENTS

Parameters	Measured values
Capacitance per finger pair (C_s)	1pF/cm
K^2 from data set with 8 μm pitch	$(0.93 \pm 0.05) \times 10^{-4}$%
K^2 from data set with 5 μm pitch	$(0.66 \pm 0.02) \times 10^{-4}$%

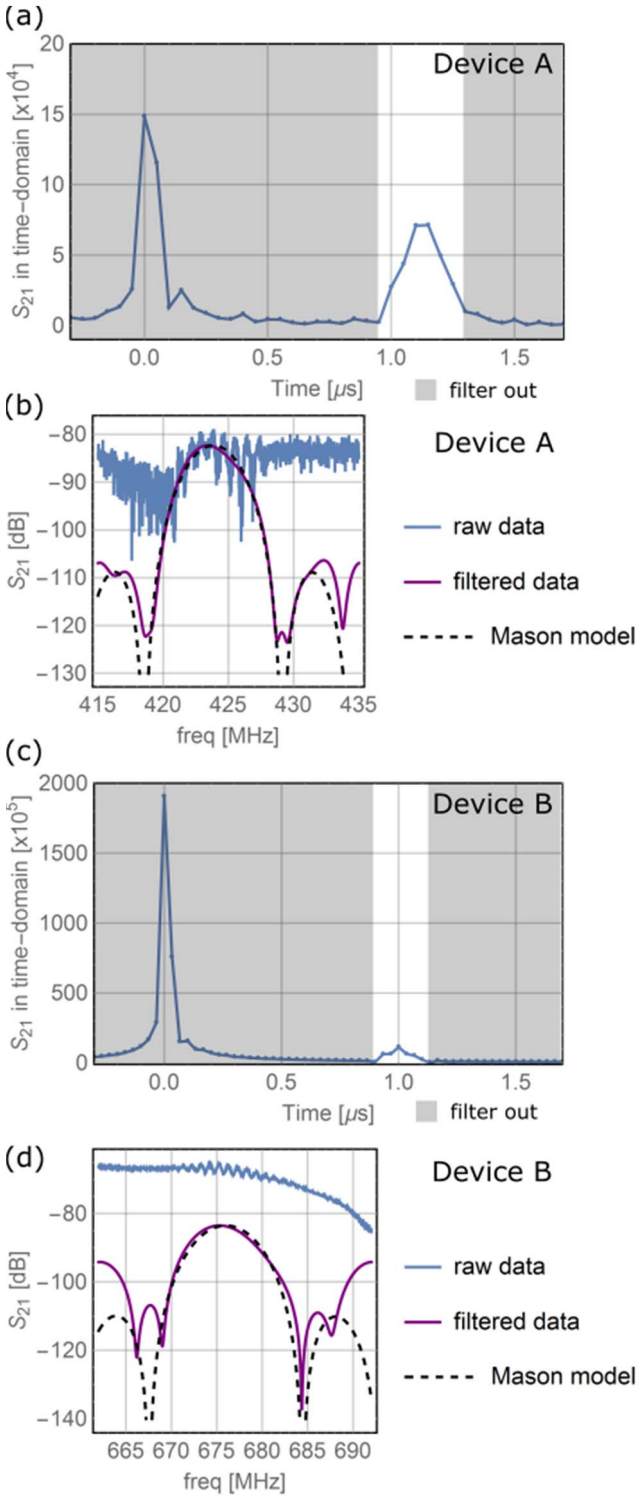

Fig. 4. Filtered signal by transforming to time domain. The plot shows the results for two devices A and B. The device parameters for A are (p, N_p, W, L_0) = (8 μm, 80, 400 μm, 400 λ). The device parameters for B are (p, N_p, W, L_0) = (5 μm, 80, 400 μm, 600 λ). (a) and (c) Time domain S_{21} for device A and B. The data in grey is filtered out. (b) and (d) Plots the raw data, filtered data, and the filtered curve based on the Mason model.

IV. DISCUSSION

We implement the measured Rayleigh wave speed, C_s, and K^2 into a 2D COMSOL simulation. We calculate that a 4H SiC delay line with a K^2 of 0.9×10^{-4} % can generate a stress of 0.5 MPa (equivalently a strain of 1×10^{-6}), and an in-plane displacement of 0.9 pm at +30 dBm RF power. A 4H SiC surface acoustic wave resonator with finesse of 100 can generate a stress of 50 MPa. This level of stress is sufficient to drive spin transition in the ground state triplet of the divacancy [12].

REFERENCES

[1] D. D. Awschalom, R. Epstein, and R. Hanson, "The diamond age of spintronics.," *Sci. Am.*, vol. 297, no. 4, pp. 84–91, 2007.

[2] S. Kolkowitz *et al.*, "Coherent sensing of a mechanical resonator with a single-spin qubit," *Science*, vol. 335, p. 1603, 2012.

[3] E. R. Macquarrie, T. A. Gosavi, N. R. Jungwirth, S. A. Bhave, and G. D. Fuchs, "Mechanical spin control of nitrogen-vacancy centers in diamond," *Phys. Rev. Lett.*, vol. 111, p. 227602, 2013.

[4] P. Ovartchaiyapong, K. W. Lee, B. A. Myers, and A. C. B. Jayich, "Dynamic strain-mediated coupling of a single diamond spin to a mechanical resonator," *Nat. Commun.*, vol. 5, p. 4429, 2014.

[5] P. Rabl, S. J. Kolkowitz, F. H. L. Koppens, J. G. E. Harris, P. Zoller, and M. D. Lukin, "A quantum spin transducer based on nanoelectromechanical resonator arrays," *Nat. Phys.*, vol. 6, no. 8, p. 602, 2010.

[6] M. J. A. Schuetz, E. M. Kessler, G. Giedke, L. M. K. Vandersypen, M. D. Lukin, and J. I. Cirac, "Universal quantum transducers based on surface acoustic waves," *Phys. Rev. X.*, vol. 5, no. 3, p. 31031, 2015.

[7] T. A. Gosavi, E. R. Macquarrie, G. D. Fuchs, and S. A. Bhave, "HBAR as a High Frequency High Stress Generator," in *Ultrasonics Symposium, 2015 IEEE*, 2015.

[8] W. F. Koehl, B. B. Buckley, F. J. Heremans, G. Calusine, and D. D. Awschalom, "Room temperature coherent control of defect spin qubits in silicon carbide," *Nat.*, vol. 479, no. 7371, p. 84, 2011.

[9] J. Van Daal, "No Title," *Philips Res. Reports*, vol. 3, p. 76, 1965.

[10] S. Karmann, R. Helbig, and R. A. Stein, "Piezoelectric properties and elastic constants of 4H and 6H SiC at temperatures 4-320 K," *J. Appl. Phys.*, vol. 66, no. 8, pp. 3922–3924, 1989.

[11] S. Ghaffari *et al.*, "Quantum Limit of Quality Factor in Silicon Micro and Nano Mechanical Resonators," *Sci. Rep.*, vol. 3, p. 3244, 2013.

[12] A. L. Falk *et al.*, "Electrically and mechanically tunable electron spins in silicon carbide color centers," *Phys. Rev. Lett.*, vol. 112, no. 18, p. 187601, 2014.

[13] S. Datta, *Surface acoustic wave devices*, 1986.

[14] Y. Takagaki, P. Santos, E. Wiebicke, O. Brandt, H.-P. Schönherr, and K. Ploog, "Guided propagation of surface acoustic waves in AlN and GaN films grown on 4H–SiC(0001) substrates," *Phys. Rev. B*, vol. 66, p. 155439, 2002.